doi: 10.18323/2782-4039-2023-3-65-2

Development and airworthiness certification of state of art additively manufactured AlSi10Mg mission critical selector valve body part for aerospace

Ponnusamy Vignesh*[1], Ph.D., Junior Specialist-1
K.V. Praveen, Bachelor of Engineering, Technical Assistant
Subbulakshmi Krishnakumar, Bachelor of Engineering, Technical Assistant
Mohanrao Chembu Bhuvaneswari, Bachelor of Engineering, Regional Director (Sc 'F')
Shirish Sharad Kale, Ph.D., Director (Sc 'G')
Theagarajan Ram Prabhu, Ph.D., Joint Director (Sc 'E')
RCMA (F&F), CEMILAC, Defence R&D Organization, Bangalore (India)

***E-mail: vigneshpt3532@gmail.com** [1]ORCID: https://orcid.org/0000-0003-4487-2030

Received 22.06.2023 *Accepted 15.08.2023*

Abstract: Aerospace applications can benefit from additive manufacturing (AM), which is highly advantageous for prototyping and rapid manufacturing. It also offers cost and weight savings, as well as integrated design capabilities. As of now, there are only a few AM standards available, many materials and equipment are involved, resulting in many variables that hinder certification and adoption. As a result, nonstandard testing is making AM in the airborne materials less appealing due to its costly and time-consuming nature. The main objective of this work is to manufacture the Selector Valve Body parts of military and civil aircraft through Laser Powder Bed Fusion (LPBF) process using AlSi10Mg powder. Further, this paper has been carried out the metallurgical properties, non-destructive and destructive testing as well as the clear explanation about the certification procedures. Moreover, this underscores the need for the developing guidelines, and standards that cover all aspects of manufacturing from design to manufacturing to operation. A comprehensive analysis from liquid penetration test shows defects are within the permissible level. In addition, it exhibits higher yield strength, ultimate strength, and elongation of (259±4) MPa, (323±4) MPa, and (12.5±1.5) % respectively, along with factual evidence that the precipitation hardened AlSi10Mg indigenously developed and produced is equal in properties to the equivalent precipitation hardening aluminium alloys produced by internationally renowned manufacturers.

Keywords: additive manufacturing; AlSi10Mg; Al alloy; precipitate hardening; development and certification.

For citation: Vignesh P., Praveen K.V., Krishnakumar S., Bhuvaneswari M.C., Kale S.S., Ram Prabhu T. Development and airworthiness certification of state of art additively manufactured AlSi10Mg mission critical selector valve body part for aerospace. *Frontier Materials & Technologies*, 2023, no. 3, pp. 19–30. DOI: 10.18323/2782-4039-2023-3-65-2.

INTRODUCTION

Aerospace, military, biomedical, and automotive parts are made of traditional high-strength aluminium alloys. There are two predominant conventional Al alloys used in aerospace: a precipitation-hardened (Al–Mg–Si) alloy and aluminium 6061 (Al6061) from the 6000 series. Laser additive manufacturing of high-performance alloys like Al6061 has gained significant interest, due to producing high-strength in lightweight structures. AlSi10Mg is a close-eutectic aluminium alloy with high melt fluidity and low shrinkage, and hence has traditionally been the most suitable for laser additive processing [1; 2]. In conventional casting (gravity casting), the hypoeutectic alloy AlSi10Mg is commonly used. Because of its lightweight and excellent mechanical properties, this alloy is widely used in the automotive and aerospace sectors. Meanwhile age hardening, Mg is crucial to its functionality because it facilitates the precipitation of the β′- and β-phases (Mg_2Si) [3; 4]. Numerous investigations have previously been conducted on the additive manufacturing (AM) produced precipitation-hardened (AlSi10Mg) alloy [5]. Generally, they address microstructure, process parameter setup, and mechanical properties, although some address heat treatment as well [6; 7]. AM Al–Si alloys are being optimised by studying their microstructural evolution as they are built, and after heat treatment [8]. Due to melt pool formation, the alloy showed "fish-scale" patterns in the directions of build, and columnar grains in the perpendicular directions [9; 10]. Grain refinement of Al–Si alloys leads to enhance mechanical properties [11]. According to [12], high cooling rates can generate fine grains Al with nano-sized Si, which has higher mechanical characteristics. AM Al–Si–Mg alloys were modified, by altering their morphology and coarsening by using a particular heat treatment [13; 14]. Al alloys after precipitation hardened, especially 6xxxx Al alloys, emerged to study comprehensively for precipitates and mechanical properties [15; 16]. It has been observed that the precipitates occurred in the following order: (Al) GP zones; β"→β'→β. In the GP zones, the clusters of Mg and Si are perfectly coherent with those of the Al matrix. The metastable (β" and β') with different Mg–Si stoichiometry, whereas stable (β) with different Mg_2Si stoichiometry [17; 18]. Peak hardening usually occurs when the GP zones coexist [19]. Aging at various temperatures resulted in varied ageing kinetics, although with equal hardness magnitudes [20]. Sha et al. [21] described a comparable precipitation sequence for Al–7Si–0.6Mg, a composition identical to alloys accessible for Powder Bed Fusion (PBF) AM. In AlSi10Mg alloys, precipitation hardening is still widely used [22]. The peak hardness throughout the ageing process, on the other hand, has seldom been documented.

Given the present relevance about AlSi10Mg alloy for Lazer Powder Bed Fusion (LPBF), a greater knowledge of the precipitation hardening on the microstructure and characteristics is necessary.

The research aim is fabricating the part through LPBF process and evaluation of material as per ASTM F3318. Mechanical properties, of heat-treated LPBF AlSi10Mg alloys (T6). The precipitate development was meticulously studied concerning better comprehension of the mechanical behaviour of the Al alloy formed by LPBF.

METHODS

Powder Details

The Aluminum powder designated (ASTM F3318) was available from Carpenter in the form of a powder (Table 1). The Al powders were gas atomised having an amorphous morphology, as shown in Fig. 1. A laser diffraction study was carried out according to ASTM B822-17, to determine the particle size distribution (PSD) of powder. Fig. 2 shows the D10, D50, and D90 particle diameters in the cumulative distribution at 10, 50, and 90 %. The powder bulk density of 2.3 g/cm^3, D10, D50, and D90 values of 29.89, 41.63, and 53.95 μm, respectively.

Parameters of Laser Powder Bed Fusion

A similar set of processing parameters is used for all parts produced by the EOS M290 machine, under an inert atmosphere. We processed the parts using aluminium-specific processing parameters, which include an Yb-fibre laser with 400 W of power, a scanning rate of 7 m/s, a layer thickness of 0.03 mm, a focus diameter of 80 to 100 mm, hatch distance 0.19 mm, and a recoater type HSS.

Heat Treatment

The body parts of the alloy produced by LPBF subjected: 1) stress relieving at 270±20 °C and soak for 90±15 min and air-cooling; 2) solutionising temperature 530±14 °C and soak for 30±10 min, followed by water quenching. Aging cycle 165±10 °C for 360±15 min followed by air-cooling.

Characterisation

The elements were analysed chemically as per ASTM E3061 using optical emission spectrometers. Microstructural characteristics and grain size were determined as per ASTM E3 & ASTM E407. X-ray radiography test performed on the body parts as per ASTM E1742/E1742M. Liquid (florescence) penetrant testing performed on the body parts as per ASTM E1417. X-ray diffraction (XRD) was carried out to measure the residual stress as per ASTM E2860 in four locations as shown in Fig. 3. In XRD experiments, the voltage, scanning rate, 2θ range, radiation type, and step size were set as 40 kV, 5 deg/min, 10–90°, Cu–Kα, and 0.028°.

Mechanical Properties

In order to test for Brinell hardness on the specimen cross-section, an ASTM E10 hardness test was performed. By applying the load at three different locations, the mean value of hardness (HBW) can be calculated. According to tensile curves, we can determine ultimate strength (UTS), yield strength (YS), and elongation. Tensile tests were conducted in all three directions (XY, Z & 45°) using an ASTM E8 standard (a sample).

RESULTS

Chemical composition

As shown in Table 2, the chemical composition of selector valve body parts, in LPBF as-build, was obtained over two samples of the AlSi10Mg alloy. Noticeably from these results, the alloy's chemical composition is within ASTM F3318 allowable limits. Additionally, oxygen, nitrogen, and hydrogen gas levels were measured and found to be 0.0862, 0.001, and 0.004 wt. %, respectively.

Microstructure of AlSi10Mg in T6 condition

The microstructure of the AlSi10Mg alloy prepared by the LPBF technique after the precipitation hardening is shown in Fig. 4. The precipitated hardened samples (Fig. 4 a), molten pool's edge was not clearly visible, and numerous tiny flakes with elliptical shapes were found on the surface. These irregular flakes, which are elliptical in shape, are scattered throughout the specimens and associate the accumulation zones of precipitates at each end of the long molten pool. This characteristic suggests that in the sample that underwent heat treatment, the precipitate's aggregation region was eroded. Precipitates it is visible in the magnified pictures (Fig. 4 b) that dispersed along the margins of the molten pool, with a limited width of band. After the precipitation hardening, elongated molten pool lost its approximately spherical precipitate bands. Precipitation hardening has significantly coarsened Si particles, which has eliminated distinctive columnar grains. Therefore, T6 heat treatment can help to attain superior mechanical properties by promoting grain refinement and homogenous microstructure.

Mechanical Properties AlSi10Mg in T6 condition

The engineering stress-strain curve showing precipitation hardening's effect on mechanical properties shown in Fig. 5. A summary of selected properties can be found in Table 3. The AlSi10Mg alloy is distinguished by high YS (259±6 MPa) and UTS (324±4 MPa) values, which are typically larger than those achieved by traditional manufacturing process.

Experimental Evaluation of the Inspection Techniques

X-ray testing, and liquid penetrant inspection were applied in order to detect the samples defects. The as-built selector value body parts are subjected to an X-ray radiography examination for the purpose of evaluating defects throughout the specimen (maximum permissible level, as shown in Table 4). The samples with LPBF have been found to be free from any visible weld defects like porosity, lack of penetration, and cracking defects.

Liquid penetrant (LP) examinations are one of the fastest and most common methods of checking LPBF inspections for discontinuities and subsurface openings. Initially, a cleaner is used to clean the surface of the samples, and then penetrant is applied and allowed to dwell for a sufficient period. In order to examine the surface of the sample,

Table 1. *Chemical composition of AlSi10Mg powder wt. %*
Таблица 1. *Химический состав порошка AlSi10Mg, мас. %*

Elements	Cu	Fe	Mg	Mn	Ni	Si	Zn	Ti	Pb	Sn	Others-total	Al
Limits	0.05 max	0.55 max	0.20–0,45	0.45 max	0.05 max	9–11	0.10 max	0.15 max	0.05 max	0.05 max	0.15 max	Bal

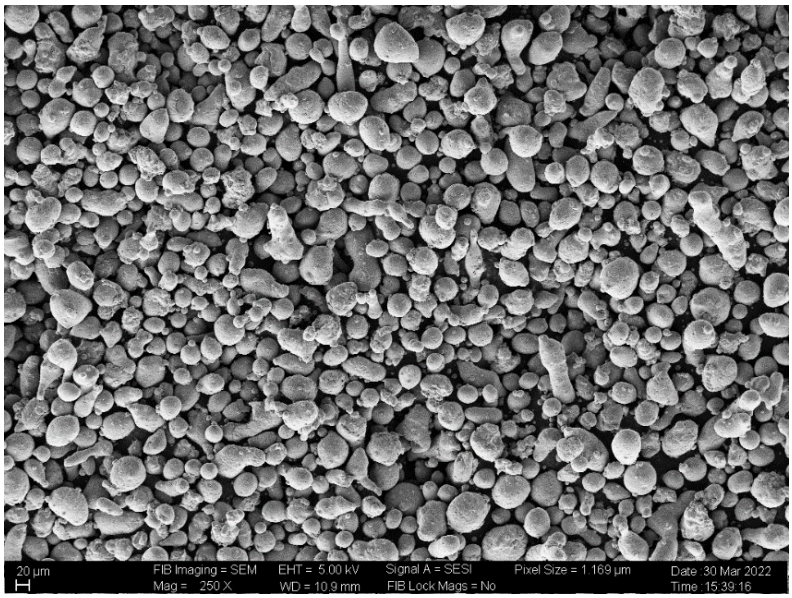

Fig. 1. *AlSi10Mg powder material as seen in SEM images*
Рис. 1. *Порошковый материал AlSi10Mg на РЭМ-изображениях*

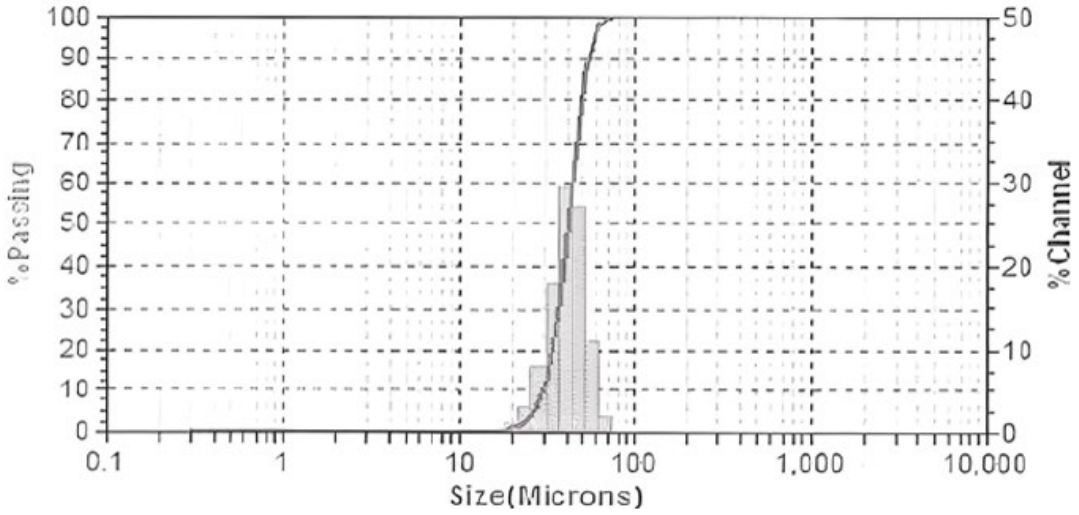

Fig. 2. *Distribution of particle sizes in AlSi10Mg powder*
Рис. 2. *Распределение по размерам частиц в порошке AlSi10Mg*

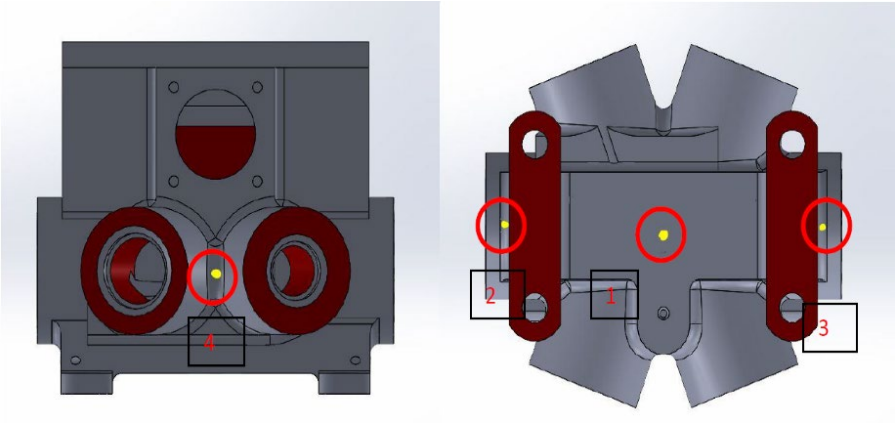

Fig. 3. *Measurement of residual stress in marked areas*
Рис. 3. *Измерение остаточного напряжения в выделенных областях*

Table 2. *Chemical composition of AlSi10Mg in as-developed condition, wt. %*
Таблица 2. *Химический состав AlSi10Mg в исходном состоянии, мас. %*

Elements	Cu	Fe	Mg	Mn	Ni	Si	Zn	Ti	Pb	Sn	Others-total	Al
Limits	0.05 max	0.55 max	0.20–0.45	0.45 max	0.05 max	9–11	0.10 max	0.15 max	0.05 max	0.05 max	0.15 max	Bal
Sample 1	0.028	0.215	0.329	0.046	0.035	10.31	0.032	0.020	0.015	0.024	0.048	Bal
Sample 2	0.032	0.223	0.327	0.046	0.036	10.21	0.035	0.020	0.016	0.024	0.048	Bal

excess penetrant must be removed from the specimen before developer is applied. As shown in Fig. 6, the selector valve body parts were fabricated by additive manufacturing. Fluorescent penetrant inspection was performed on these parts to verify that they met the acceptance criteria listed in Table 5. The selector value body parts were subjected to a liquid penetrant examination. There are no indications of discrete cracks or microcracks on the surfaces of the AM parts. A noteworthy feature of the surface is the absence of inclusions, stringers, cracks, seams, laps, undercuts, flakes, and laminations. As far as airworthiness is concerned, the two non-destructive tests listed above are of great importance. The selector valve body parts cannot be deployed in the hydraulic system if they fail these two tests.

Residual stress

The residual stress of AlSi10Mg in the T6 condition is shown in Fig. 7. There are different points at which residual stress measurements can be made, so a residual stress value is the average of them all. As a result of plastic deformation, materials usually generate residual stresses. In spite of this, no plastic deformation has occurred in the LPBF specimens. A repeating rapid heating and cooling of the molten phase accumulates residual thermal stresses in the solidified layer. The specimen 1 is clearly subjected to compressive residual stress (location 1), which gradually increases (locations 2 and 3). The specimen 1 is clearly subjected to compressive residual stress (location 1), which gradually increases (locations 2 and 3). In contradictory location 4, the residual stress turns into tensile stress. Specimen 2 is initially subjected to compressive stress, steep increases in residual stress, which turned into a tensile test in location 2, and then back to compressive stress in locations 3 and 4.

Airworthiness certification

This section describes the typical airworthiness certification (AWC) process of aerospace LPBF with an example of selector valve body parts. AWC of Selector Valve Body Parts LPBF has three phases: (1) process design evaluation, (2) development trials and testing, and (3) certification documentation.

The component under examination is categorized for functionality and process criticality while evaluating process designs. In the current study, selector valve body parts that are typically modelled before beginning trials were examined. In the model, the component is LPBF for various process parameter combinations and is analysed for the degree of ease and comfort in the LPBF contours and sharp information, as well as the defect evolution. After finalising the process parameters, trials simulate the modelling constraints to verify the model's accuracy. Following that, airworthiness authorities review and certify the design

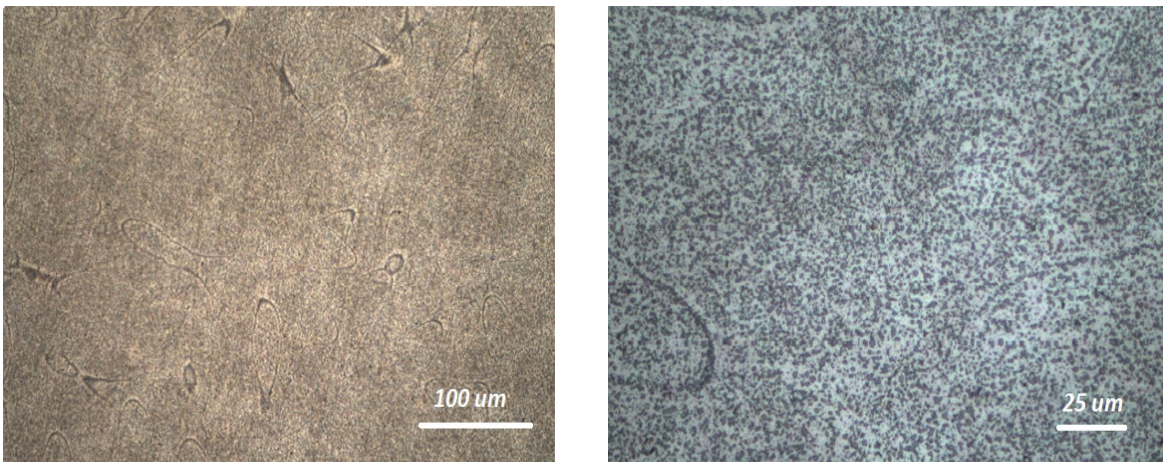

a *b*

Fig. 4. *Optical microstructure of AlSi10Mg at T6 condition* ***(a)*** *and higher magnification* ***(b)***
Рис. 4. *Оптическое изображение микроструктуры AlSi10Mg в режиме T6* ***(а)*** *и увеличенное изображение* ***(b)***

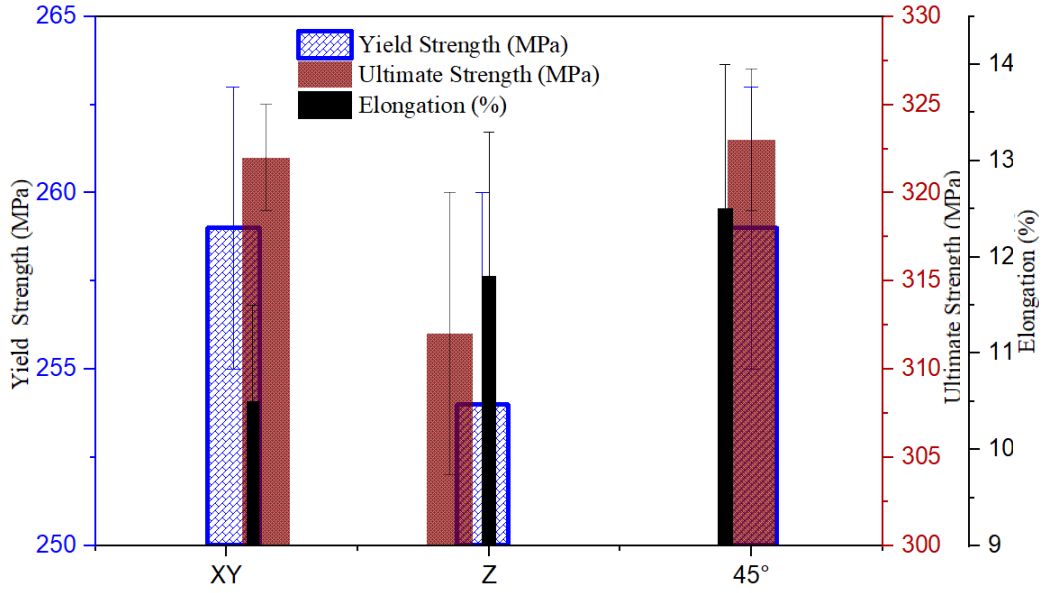

Fig. 5. *Tensile properties of T6 condition AlSi10Mg test samples*
Рис. 5. *Свойства при растяжении испытательных образцов AlSi10Mg в режиме T6*

Table 3. *Mechanical properties of selector valve body parts in T6 conditions*
Таблица 3. *Механические свойства деталей корпуса переключателя в режиме T6*

Specimen direction	Yield Strength, MPa	Ultimate Strength, MPa	Elongation, %	Hardness, HBW
XY	259±4	322±3	10.5±1	88.8±2
Z	254±6	312±8	11.8±1.5	
45°	259±4	323±4	12.5±1.5	

Table 4. *Maximum permissible radiography severity levels for discontinuity*
Таблица 4. *Максимально допустимые уровни радиографической интенсивности для неоднородности*

Discontinuity	Severity Level – Grade B	
	¼	¾
Gas Holes	1	1
Gas Porosity, Round	1	1
Gas Porosity, Elongated	1	2
Foreign Material	1	1
Keyhole porosity	<0.152 mm	
Cracks	None	
Surface irregularity	Not to exceed drawing tolerance	
Overlaps	None	
Incomplete Fusion	None	

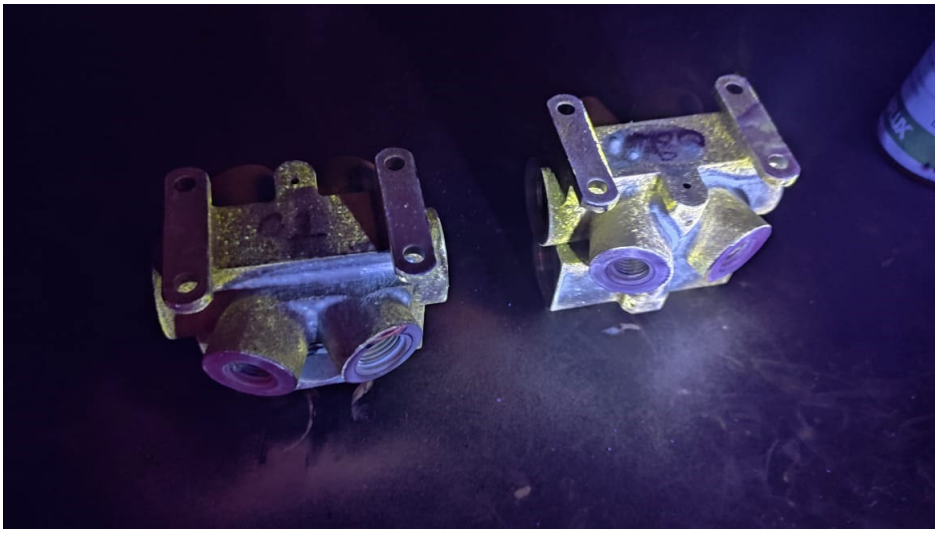

Fig. 6. *Result Dye penetrant test of selector valve body parts*
Рис. 6. *Результат цветной дефектоскопии деталей корпуса переключателя*

parameters. Finally, the drawing, and design validation report are developed and subjected to airworthiness qualification testing. Additionally, the qualification tests necessary to verify the airworthiness of Selector valve body parts are created based on the components functioning, operating conditions, and interactions with other parts. In this example, selector valve body parts (LPBF) have been subjected to post-heat treatment, during which, structure property correlations were carried out. Selector valve body components are a line replaceable unit (LRU), thus the fault tolerance level is extremely restrictive since any flaws larger than the critical size seriously impair hydraulic system performance. As a standard practise for surface defect inspection, radiography testing (ASTM E1742) and fluorescence penetrant inspection (ASTM E1417) are recommended.

A thorough test plan that includes testing requirements in accordance with aerospace material and testing standards, component geometry, and designer-specific testing needs, is created based on the aforementioned inputs, and certified by airworthiness agencies. The sample strategy is designed, based on the testing method, designer specifications, and part criticality. Non-destructive and destructive testing are typically performed on a single sample per batch and in parts produced. The qualification of the test schedule of the LPBF in the presence of airworthiness agencies is carried out in development batches. After testing,

Table 5. *Maximum discontinuity sizes (in mm) and distributions are allowed*
Таблица 5. *Максимальные допустимые размеры (в мм) и распределения неоднородностей*

Type of discontinuity	Max size of discontinuity allowed
Inclusion rounded: surface	1.193 dia D-3*
Inclusion rounded: subsurface	1.6 dia D-3*
Inclusion stringers: surface	9.52 long DD-1**
Inclusion stringers: subsurface	12.7 long DD-1**
Laps or seams (unmachined surfaces)	25.4 long DD-1**
Laps or seams or (machined surfaces)	0
Propagating discontinuities (laminations, flakes, cracks, etc.)	0
Unmelted particle, balling, porosity	None

Note. The following is a list of distribution designations.
** D-3 – there should be no more than three times the maximum distance between discontinuities.*
*** DD-1 – linear discontinuities cannot be closer than 12.7 mm and parallel discontinuities cannot be closer than 6.35 mm.*
*Примечание. * D-3 – между неоднородностями должно быть не более трех максимальных расстояний.*
*** DD-1 – расстояние между линейными неоднородностями не может быть меньше, чем 12,7 мм, а между параллельными неоднородностями – меньше, чем 6,35 мм.*

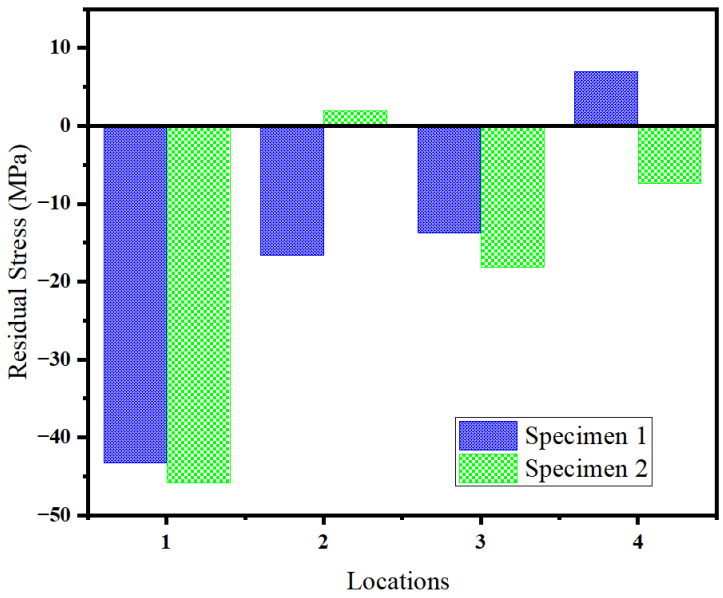

Fig. 7. *Residual stress in precipitation hardened AlSi10Mg specimens*
Рис. 7. *Остаточное напряжение в образцах дисперсионно-твердеющего AlSi10Mg*

the reports are prepared and submitted to airworthiness agencies for review.

Before certification by airworthiness agencies, the testing reports are rigorously checked and validated for correctness in the final step of certification which is shown in the Fig. 8. Following a thorough review of the reports, Selector valve body parts is granted permission to continue manufacturing on the specific platform. Part machining, fitting, functional tests simulating real hydraulic operating conditions, and prototype hydraulic units trials are all part of the selector valve body parts.

Certification includes the process and product validation against the test schedule. The tests that must be performed to qualify the Selector valve body components are determined by the material specification and operating conditions. Working conditions include things like operational temperature and contact condition. The following tests must be performed in order to certify

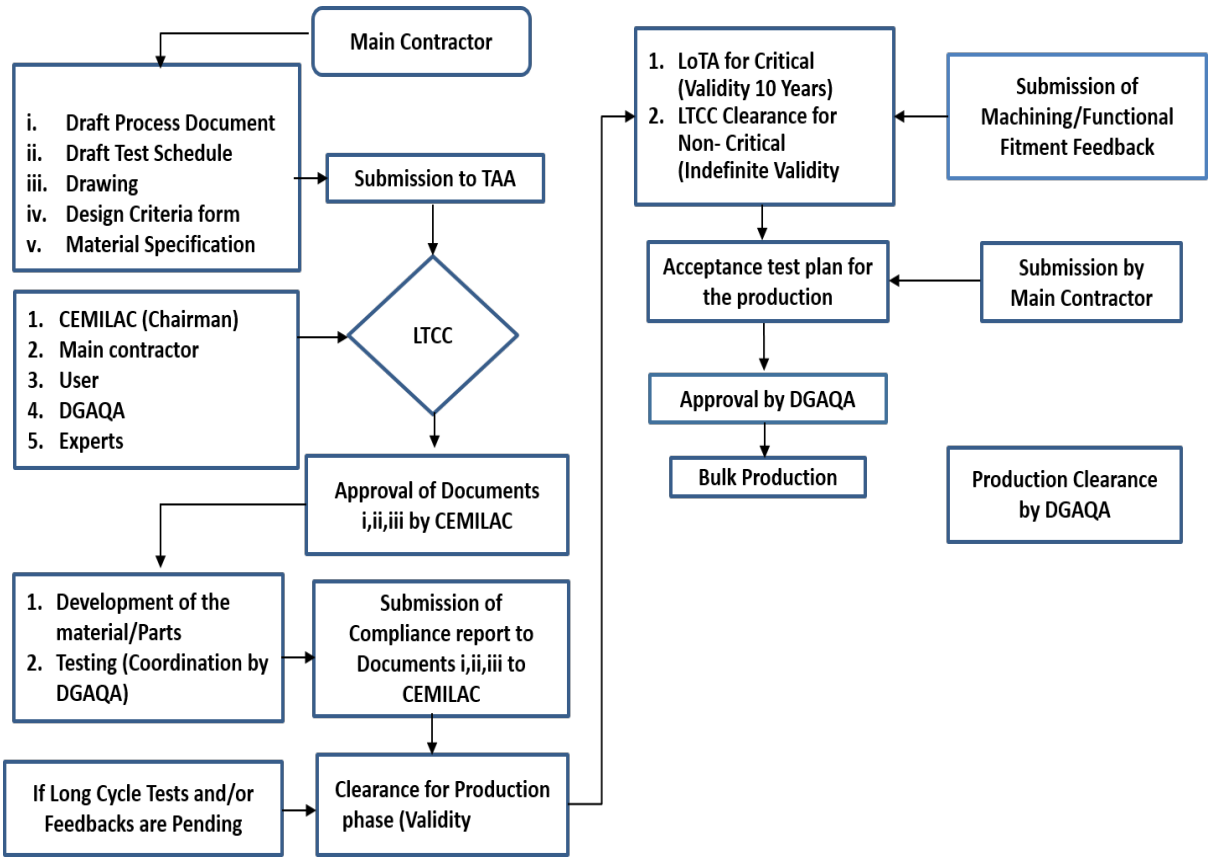

Fig. 8. *An overview of the certification process*
Рис. 8. *Общее представление процесса сертификации*

the process and product: (1) chemical composition to correspond to the material specification; (2) NDT (X-ray and Dye penetrant testing) to validate the defect level within a reasonable range; (3) microstructure to confirm the heat treatment procedure; and (4) a tensile test at room temperature on a specimen in the independently required condition.

The foregoing tests are performed, and the test reports are checked for conformity to the AM (LPBF) test schedule. These are provisionally certified for component-level LRU performance based on good compliance. Following successful completion of the aforesaid tests, the selector valve body parts is type certified for five years by the Indian military airworthiness certification organization (CEMILAC).

DISCUSSION

The alloy's extremely fine grains microstructure, which is developed by rapid solidification. On the other hand, AM parts have low elongation (12.5 %). A material's strength significantly enhanced by the formation and homogenous distribution of precipitates due to artificial aging. During the aging process, precipitation occurs as a result of the reaction of Mg with Si, where fine grains of precipitate interact with dislocations which leads to strengthening of the material. The precipitation hardening process involves several stages. As a first step, Mg and Si atoms form small clusters (GP zones). Mg_2Si then precipitates nucleate in metastable and coherent β″ phases. These progressively transition into metastable and semi coherent β′ phases, which have the greatest strengthening effect. As-fabricated LPBF samples are generally much harder than heat-treated T4 materials. In T4 conditions fine-grained recrystallisation microstructure created during a solid solution is the cause of this reduced hardness. LPBF specimen can exhibit high hardness values due to their cellular dendritic microstructures, dislocation structures, and fine dispersion of eutectic Si in the Al matrix [12]. The solutionising treatment, on the other hand, dissolves these secondary phases and significantly reduces hardness [13], the following artificial ageing can cause metastable phases such as Mg_2Si precipitate. This change may have a minor impact on the hardness values. As a result, the precipitation hardening has an effect on increasing hardness, however, it may be necessary to reduce stress and obtain other mechanical qualities. As a result of plastic deformation, materials usually generate residual stresses. In spite of this, no plastic deformation has occurred in the LPBF specimens. A repeating rapid heating and cooling of the molten phase accumulates residual thermal stresses in the solidified layer. Laser beams can result in complex stresses on specimens during Laser Additive Manufacturing (LAM), processing because the underlying layer is remelted and reheated. Heat gradients along the building direction cause alternating tensile and compressive residual stresses between the underlying and

subsequent layers. Because of the large scale and low quantity of grain boundaries in the T6 specimen, dislocations glide and climb easily (Fig. 4). In order to improve mechanical properties and increase service life, tensile residual stress must be reduced or eliminated from a material.

CONCLUSIONS

LPBF has been used for the development and testing of selector valve body parts, and the process is well suited to fabricate selector valve body parts using additive manufacturing. The preferred material for selector valve body parts is AlSi10Mg. There have been discussions regarding the potential application of different service areas throughout the AM process, including design, materials, pre-processing, 3D-printing and manufacturing, post-processing, testing and inspection, verification, and certification. This novel certification pathway will provide the hydraulic system of aircraft and its supply chain ecosystem, with a novel approach to identify the most efficient path to building trust and confidence in the adoption of this emerging technology, which would otherwise not be possible because of its novel approach.

REFERENCES

1. Bradford R.L., Cao L., Klosterman D., Herman F., Forman L., Browning C. A metal–metal powder formulation approach for laser additive manufacturing of difficult-to-print high-strength aluminum alloys. *Materials Letters*, 2021, vol. 300, article number 130113. DOI: 10.1016/j.matlet.2021.130113.
2. Bajakke P.A., Malik V.R., Deshpande A.S. Particulate metal matrix composites and their fabrication via friction stir processing – a review. *Materials and Manufacturing Processes*, 2018, vol. 34, no. 8, pp. 833–881. DOI: 10.1080/10426914.2019.1605181.
3. Matilainen V., Piili H., Salminen A., Syvänen T., Nyrhilä O. Characterization of process efficiency improvement in laser additive manufacturing. *Physics Procedia*, 2014, vol. 56, pp. 317–326. DOI: 10.1016/j.phpro.2014.08.177.
4. Fousová M., Dvorský D., Michalcová A., Vojtěch D. Changes in the microstructure and mechanical properties of additively manufactured AlSi10Mg alloy after exposure to elevated temperatures. *Materials Characterization*, 2018, vol. 137, pp. 119–126. DOI: 10.1016/j.matchar.2018.01.028.
5. Tradowsky U., White J., Ward R.M., Read N., Reimers W., Attallah M.M. Selective laser melting of AlSi10Mg: Influence of post-processing on the microstructural and tensile properties development. *Materials & Design*, 2016, vol. 105, pp. 212–222. DOI: 10.1016/j.matdes.2016.05.066.
6. Zhou L., Mehta A., Schulz E., McWilliams B., Cho K., Sohn Y. Microstructure, precipitates and hardness of selectively laser melted AlSi10Mg alloy before and after heat treatment. *Materials Characterization*, 2018, vol. 143, pp. 5–17. DOI: 10.1016/j.matchar.2018.04.022.
7. Li X.P., Wang X.J., Saunders M., Suvorova A., Zhang L.C., Liu Y.J., Fang M.H., Huang Z.H., Sercombe T.B. A selective laser melting and solution heat treatment refined Al–12Si alloy with a controllable ultrafine eutectic microstructure and 25% tensile ductility. *Acta Materialia*, 2015, vol. 95, pp. 74–82. DOI: 10.1016/j.actamat.2015.05.017.
8. Andersen S.J., Zandbergen H.W., Jansen J., TrÆholt C., Tundal U., Reiso O. The crystal structure of the β″phase in Al–Mg–Si alloys. *Acta Materialia*, 1998, vol. 46, no. 9, pp. 3283–3298. DOI: 10.1016/S1359-6454(97)00493-X.
9. Rometsch P.A., Schaffer G.B. An age hardening model for Al–7Si–Mg casting alloys. *Materials Science and Engineering: A*, 2002, vol. 325, no. 1-2, pp. 424–434. DOI: 10.1016/S0921-5093(01)01479-4.
10. Montero-Sistiaga M.L., Mertens R., Vrancken B., Wang X., Van Hooreweder B., Kruth J.P., Van Humbeeck J. Changing the alloy composition of Al7075 for better processability by selective laser melting. *Journal of Materials Processing Technology*, 2016, vol. 238, pp. 437–445. DOI: 10.1016/j.jmatprotec.2016.08.003.
11. Li W., Li S., Liu J., Zhang A., Zhou Y., Wei Q., Yan C., Shi Y. Effect of heat treatment on AlSi10Mg alloy fabricated by selective laser melting: Microstructure evolution, mechanical properties and fracture mechanism. *Materials Science and Engineering: A*, 2016, vol. 663, pp. 116–125. DOI: 10.1016/j.msea.2016.03.088.
12. Takata N., Kodaira H., Sekizawa K., Suzuki A., Kobashi M. Change in microstructure of selectively laser melted AlSi10Mg alloy with heat treatments. *Materials Science and Engineering: A*, 2017, vol. 704, pp. 218–228. DOI: 10.1016/j.msea.2017.08.029.
13. Reunova K.A., Astafurova E.G., Moskvina V.A., Astafurov S.V., Panchenko M.Y., Melnikov E.V., Kolubaev E.A. Microstructure and Phase Composition of a Gradient Material "Stainless Steel/Cr-Ni Alloy" Produced by Electron-Beam Additive Manufacturing. *Russian Physics Journal*, 2022, vol. 65, pp. 771–777. DOI: 10.1007/s11182-022-02696-0.
14. Astafurova E.G., Panchenko M.Yu., Moskvina V.A. et al. Microstructure and grain growth inhomogeneity in austenitic steel produced by wire-feed electron beam melting: The effect of post-building solid-solution treatment. *Journal of Materials Science*, 2020, vol. 55, no. 22, pp. 9211–9224. DOI: 10.1007/s10853-020-04424-w.
15. Moskvina V.A., Melnikov E.V., Zagibalova E.A. Characteristics of a gradient material based on chromium-nickel stainless steel and Cr20Ni80 alloy produced by electron-beam 3D-printing. *Vektor nauki Tolyattinskogo gosudarstvennogo universiteta*, 2021, no. 3, pp. 57–66. DOI: 10.18323/2073-5073-2021-3-57-66.
16. Khalikova G.R., Zakirova G.R., Farkhutdinov A.I., Korznikova E.A., Trifonov V.G. The structure and mechanical properties of the AK12D (Al-Si-Cu-Ni-Mg) aluminum alloy subjected to friction stir processing. *Frontier Materials & Technologies*, 2022, no. 3-2, pp. 99–108. DOI: 10.18323/2782-4039-2022-3-2-99-108.

17. Torubarov I.S., Drobotov A.V., Gushchin I.A., Vdovin D.S., Plotnikov A.L., Yakovlev A.A. Additive manufacturing of parts with three-dimensional continuous fiber reinforcement. *Frontier Materials & Technologies*, 2022, no. 2, pp. 92–104. DOI: 10.18323/2782-4039-2022-2-92-104.
18. Vetkasov N.I., Kapustin A.I., Sapunov V.V. The development and application of the process of preliminary formation of the high-homogeneous dry mixture “Aluminum powder – single-wall CNT” in the technology ofproduction of the aluminium matrix composites. *Vektor nauki Tolyattinskogo gosudarstvennogo universiteta*, 2018, no. 3, pp. 14–21. DOI: 10.18323/2073-5073-2018-3-14-21.
19. Raja A., Cheethirala S.R., Gupta P., Vasa N.J., Jayaganthan R. A review on the fatigue behaviour of AlSi10Mg alloy fabricated using laser powder bed fusion technique. *Journal of Materials Research and Technology*, 2022, vol. 17, pp. 1013–1029. DOI: 10.1016/j.jmrt.2022.01.028.
20. Limbasiya N., Jain A., Soni H., Wankhede V., Krolczyk G., Sahlot P. Comprehensive review on the effect of process parameters and post-process treatments on microstructure and mechanical properties of selective laser melting of AlSi10Mg. *Journal of Materials Research and Technology*, 2022, vol. 21, pp. 1141–1176. DOI: 10.1016/j.jmrt.2022.09.092.
21. Sha G., Möller H., Stumpf W.E., Xia J.H., Govender G., Ringer S.P. Solute nanostructures and their strengthening effects in Al–7Si–0.6 Mg alloy F357. *Acta Materialia*, 2012, vol. 60, no. 2, pp. 692–701. DOI: 10.1016/j.actamat.2011.10.029.
22. Zhao L., Song L., Macías J.G.S., Zhu Y., Huang M., Simar A., Li Z. Review on the correlation between microstructure and mechanical performance for laser powder bed fusion AlSi10Mg. *Additive Manufacturing*, 2022, vol. 56, article number 102914. DOI: 10.1016/j.addma.2022.102914.

СПИСОК ЛИТЕРАТУРЫ

1. Bradford R.L., Cao L., Klosterman D., Herman F., Forman L., Browning C. A metal–metal powder formulation approach for laser additive manufacturing of difficult-to-print high-strength aluminum alloys // Materials Letters. 2021. Vol. 300. Article number 130113. DOI: 10.1016/j.matlet.2021.130113.
2. Bajakke P.A., Malik V.R., Deshpande A.S. Particulate metal matrix composites and their fabrication via friction stir processing – a review // Materials and Manufacturing Processes. 2018. Vol. 34. № 8. P. 833–881. DOI: 10.1080/10426914.2019.1605181.
3. Matilainen V., Piili H., Salminen A., Syvänen T., Nyrhilä O. Characterization of process efficiency improvement in laser additive manufacturing // Physics Procedia. 2014. Vol. 56. P. 317–326. DOI: 10.1016/j.phpro.2014.08.177.
4. Fousová M., Dvorský D., Michalcová A., Vojtěch D. Changes in the microstructure and mechanical properties of additively manufactured AlSi10Mg alloy after exposure to elevated temperatures // Materials Characterization. 2018. Vol. 137. P. 119–126. DOI: 10.1016/j.matchar.2018.01.028.
5. Tradowsky U., White J., Ward R.M., Read N., Reimers W., Attallah M.M. Selective laser melting of AlSi10Mg: Influence of post-processing on the microstructural and tensile properties development // Materials & Design. 2016. Vol. 105. P. 212–222. DOI: 10.1016/j.matdes.2016.05.066.
6. Zhou L., Mehta A., Schulz E., McWilliams B., Cho K., Sohn Y. Microstructure, precipitates and hardness of selectively laser melted AlSi10Mg alloy before and after heat treatment // Materials Characterization. 2018. Vol. 143. P. 5–17. DOI: 10.1016/j.matchar.2018.04.022.
7. Li X.P., Wang X.J., Saunders M., Suvorova A., Zhang L.C., Liu Y.J., Fang M.H., Huang Z.H., Sercombe T.B. A selective laser melting and solution heat treatment refined Al–12Si alloy with a controllable ultrafine eutectic microstructure and 25% tensile ductility // Acta Materialia. 2015. Vol. 95. P. 74–82. DOI: 10.1016/j.actamat.2015.05.017.
8. Andersen S.J., Zandbergen H.W., Jansen J., TrÆholt C., Tundal U., Reiso O. The crystal structure of the β″ phase in Al–Mg–Si alloys // Acta Materialia. 1998. Vol. 46. № 9. P. 3283–3298. DOI: 10.1016/S1359-6454(97)00493-X.
9. Rometsch P.A., Schaffer G.B. An age hardening model for Al–7Si–Mg casting alloys // Materials Science and Engineering: A. 2002. Vol. 325. № 1-2. P. 424–434. DOI: 10.1016/S0921-5093(01)01479-4.
10. Montero-Sistiaga M.L., Mertens R., Vrancken B., Wang X., Van Hooreweder B., Kruth J.P., Van Humbeeck J. Changing the alloy composition of Al7075 for better processability by selective laser melting // Journal of Materials Processing Technology. 2016. Vol. 238. P. 437–445. DOI: 10.1016/j.jmatprotec.2016.08.003.
11. Li W., Li S., Liu J., Zhang A., Zhou Y., Wei Q., Yan C., Shi Y. Effect of heat treatment on AlSi10Mg alloy fabricated by selective laser melting: Microstructure evolution, mechanical properties and fracture mechanism // Materials Science and Engineering: A. 2016. Vol. 663. P. 116–125. DOI: 10.1016/j.msea.2016.03.088.
12. Takata N., Kodaira H., Sekizawa K., Suzuki A., Kobashi M. Change in microstructure of selectively laser melted AlSi10Mg alloy with heat treatments // Materials Science and Engineering: A. 2017. Vol. 704. P. 218–228. DOI: 10.1016/j.msea.2017.08.029.
13. Reunova K.A., Astafurova E.G., Moskvina V.A., Astafurov S.V., Panchenko M.Y., Melnikov E.V., Kolubaev E.A. Microstructure and Phase Composition of a Gradient Material “Stainless Steel/Cr-Ni Alloy” Produced by Electron-Beam Additive Manufacturing // Russian Physics Journal. 2022. Vol. 65. P. 771–777. DOI: 10.1007/s11182-022-02696-0.
14. Astafurova E.G., Panchenko M.Yu., Moskvina V.A. et al. Microstructure and grain growth inhomogeneity in austenitic steel produced by wire-feed electron beam melting: The effect of post-building solid-solution

treatment // Journal of Materials Science. 2020. Vol. 55. № 22. P. 9211–9224. DOI: 10.1007/s10853-020-04424-w.
15. Москвина В.А., Мельников Е.В., Загибалова Е.А. Особенности градиентного материала на основе нержавеющей хромоникелевой стали и сплава Х20Н80, изготовленного методом электронно-лучевой 3D-печати // Вектор науки Тольяттинского государственного университета. 2021. № 3. С. 57–66. DOI: 10.18323/2073-5073-2021-3-57-66.
16. Халикова Г.Р., Закирова Г.Р., Фархутдинов А.И., Корзникова Е.А., Трифонов В.Г. Структура и механические свойства алюминиевого сплава АК12Д, подвергнутого обработке трением с перемешиванием // Frontier Materials & Technologies. 2022. № 3-2. С. 99–108. DOI: 10.18323/2782-4039-2022-3-2-99-108.
17. Торубаров И.С., Дроботов А.В., Гущин И.А., Вдовин Д.С., Плотников А.Л., Яковлев А.А. Аддитивное производство изделий с пространственным армированием непрерывным волокном // Frontier Materials & Technologies. 2022. № 2. С. 92–104. DOI: 10.18323/2782-4039-2022-2-92-104.
18. Веткасов Н.И., Капустин А.И., Сапунов В.В. Разработка и применение процесса предварительного формирования высокооднородной сухой смеси «Алюминиевый порошок – одностенные УНТ» в технологии получения алюмоматричных композитов // Вектор науки Тольяттинского государственного университета. 2018. № 3. С. 14–21. DOI: 10.18323/2073-5073-2018-3-14-21.
19. Raja A., Cheethirala S.R., Gupta P., Vasa N.J., Jayaganthan R. A review on the fatigue behaviour of AlSi10Mg alloy fabricated using laser powder bed fusion technique // Journal of Materials Research and Technology. 2022. Vol. 17. P. 1013–1029. DOI: 10.1016/j.jmrt.2022.01.028.
20. Limbasiya N., Jain A., Soni H., Wankhede V., Krolczyk G., Sahlot P. Comprehensive review on the effect of process parameters and post-process treatments on microstructure and mechanical properties of selective laser melting of AlSi10Mg // Journal of Materials Research and Technology. 2022. Vol. 21. P. 1141–1176. DOI: 10.1016/j.jmrt.2022.09.092.
21. Sha G., Möller H., Stumpf W.E., Xia J.H., Govender G., Ringer S.P. Solute nanostructures and their strengthening effects in Al–7Si–0.6 Mg alloy F357 // Acta Materialia. 2012. Vol. 60. № 2. P. 692–701. DOI: 10.1016/j.actamat.2011.10.029.
22. Zhao L., Song L., Macías J.G.S., Zhu Y., Huang M., Simar A., Li Z. Review on the correlation between microstructure and mechanical performance for laser powder bed fusion AlSi10Mg // Additive Manufacturing. 2022. Vol. 56. Article number 102914. DOI: 10.1016/j.addma.2022.102914.

Разработка и сертификация летной годности современной ответственной детали корпуса переключателя для аэрокосмических систем, изготовленной из сплава AlSi10Mg с помощью аддитивной технологии

Вигнеш Поннусами*[1], доктор наук, младший специалист-1
Правин К.В., бакалавр технических наук, технический помощник
Кришнакумар Суббулакшми, бакалавр технических наук, технический помощник
Бхуванесвари Моханрао Чембу, бакалавр технических наук, региональный директор (сектор ‘F’)
Кейл Шириш Шарад, доктор наук, директор (сектор ‘G’)
Рам Прабху Тэгараджан, доктор наук, содиректор (сектор ‘E’)
Региональный центр военной полетопригодности (F&F), Центр боевой полетопригодности и сертификации, Организация оборонных исследований и разработок, Бангалор (Индия)

***E-mail: vigneshpt3532@gmail.com**

[1]ORCID: https://orcid.org/0000-0003-4487-2030

Поступила в редакцию 22.06.2023 *Принята к публикации 15.08.2023*

Аннотация: Аддитивные технологии (АТ) очень эффективны для макетирования и быстрого производства, поэтому их применение выгодно для аэрокосмической отрасли. Они позволяют сэкономить средства, а также облегчить конструкции, подходят для комплексного проектирования. Однако на данный момент доступно лишь несколько стандартов аддитивных технологий, требуется много материалов и оборудования, что приводит к возникновению затруднений с сертификацией и внедрением АТ. Нестандартные испытания приводят к тому, что АТ в аэрозольных материалах оказываются менее привлекательными из-за их дороговизны и трудоемкости. Целью работы является изготовление деталей корпуса переключателя военных и гражданских самолетов методом лазерного сплавления порошкового слоя (LPBF) с применением порошка AlSi10Mg. Выявлены физико-химические свойства материала, проведены неразрушающие и разрушающие испытания, а также даны четкие разъяснения процедур сертификации. Сделан упор на необходимости разработки руководств и стандартов, охватывающих все аспекты производства – от проектирования до изготовления и эксплуатации продукта. Комплексный анализ испытаний на проникновение жидкости показывает, что дефекты находятся в пределах допустимого уровня. AlSi10Mg демонстрирует более высокие показатели предела текучести, предела прочности и относительного

удлинения, равные (259±4) МПа, (323±4) МПа и (12,5±1,5) % соответственно. Показано, что дисперсионно-твердеющий AlSi10Mg, разработанный и производящийся в Индии, по свойствам не уступает аналогичным дисперсионно-твердеющим алюминиевым сплавам всемирно известных производителей.

Ключевые слова: аддитивное производство; AlSi10Mg; алюминиевый сплав; дисперсионное твердение; разработка и сертификация.

Для цитирования: Вигнеш П., Правин К.В., Кришнакумар С., Бхуванесвари М.Ч., Кейл Ш.Ш., Рам Прабху Т. Разработка и сертификация летной годности современной ответственной детали корпуса переключателя для аэрокосмических систем, изготовленной из сплава AlSi10Mg с помощью аддитивной технологии // Frontier Materials & Technologies. 2023. № 3. С. 19–30. DOI: 10.18323/2782-4039-2023-3-65-2.